



Seismic and geodetic constraints on Cascadia slow slip

Aaron G. Wech,¹ Kenneth C. Creager,¹ and Timothy I. Melbourne²

Received 11 September 2008; revised 6 June 2009; accepted 23 July 2009; published 31 October 2009.

[1] Automatically detected and located tremor epicenters from episodic tremor and slip (ETS) episodes in northern Cascadia provide a high-resolution map of Washington's slow slip region. Thousands of epicenters from the past four ETS events from 2004 to 2008 provide detailed map-view constraints that correlate with geodetic estimates of the simultaneous slow slip. Each of these ETS events exhibits remarkable similarity in the timing and geographic distribution of tremor density and geodetically inferred slip. Analysis of the latest 15-month inter-ETS period also reveals ageodetic tremor activity similar both in duration and extent to ETS tremor. Epicenters from both ETS and inter-ETS tremor are bounded between the 30- and 45-km plate interface depth contours and locate approximately 75 km east of previous estimates of the locked portion of the subducting Juan de Fuca plate. Inter-ETS tremor overlaps but is generally downdip of ETS tremor and does not yet correlate with geodetically observed slip, but this is likely because the slip is below current GPS detection levels. Based on the tremor and slip correlation and the tremor-duration and slip magnitude relationship, we suggest that the well-resolved, sharp updip edge of tremor epicenters reflects a change in plate interface coupling properties. The region updip of this boundary may accumulate stress with the potential for coseismic shear failure during a megathrust earthquake. Alternatively, plate convergence in this region could be accommodated by continuous slow slip with no detectable tremor or by slow slip events with sufficiently long recurrence intervals that none have been detected during the past 10 years of GPS observations.

Citation: Wech, A. G., K. C. Creager, and T. I. Melbourne (2009), Seismic and geodetic constraints on Cascadia slow slip, *J. Geophys. Res.*, 114, B10316, doi:10.1029/2008JB006090.

1. Introduction

[2] The region of Cascadia extending from northern California to northern Vancouver Island is tectonically characterized by the subduction of the oceanic Juan de Fuca plate beneath the continental North American plate. Geodetically inferred long-term deformation suggests strain accumulation in the overriding crust in response to the steady convergence of the subducting slab [McCaffrey *et al.*, 2007]. This deformation results from interseismic coupling along an offshore portion of the subducting plate interface, which is known to have exhibited multiple incidents of shear failure in the form of megathrust earthquakes up to magnitude 9 [Satake *et al.*, 2003; Goldfinger *et al.*, 2003]. Somewhere downdip of this seismogenic coupling and a zone of transition, however, the pressure, temperature, composition, and/or fluid environment at the plate interface enables the oceanic plate to freely subduct without any seismogenic coupling to the overriding continent. It is

poorly understood, though, how and where this transition is realized. As a spatially constrainable mechanism for stable strain release, episodic tremor and slip (ETS) provides information about this transition region.

[3] ETS in northern Cascadia is characterized by the repeated coincidence of seismically observed deep nonvolcanic tremor [Obara, 2002] and geodetically observed slow slip [Dragert *et al.*, 2001] every 15 ± 2 months [Miller *et al.*, 2002; Rogers and Dragert, 2003]. GPS observations provide evidence of periodic reversals from the ambient direction of relative plate motion suggesting fault slip along the subducting plate interface. Coincident with these innocuous events, seismically detected tremor is observed to correlate both spatially and temporally [Rogers and Dragert, 2003]. These tremors are characterized by a lack of high frequency content relative to normal earthquakes of similar size [Obara, 2002], which suggests that slip results from a slow, low stress-drop process, possibly associated with high pore fluid pressure [Kodaira *et al.*, 2004; Kao *et al.*, 2005; Shelly *et al.*, 2006].

[4] Each episode, lasting days to weeks, is observed to yield 2–3 cm [Szeliga *et al.*, 2008] of the 4 cm/a north-easterly convergence [Wilson, 1993] of the subducting Juan de Fuca plate beneath North America. These events reduce the moment available for high-stress-drop failure in the slow slip region and may hold the key for better understanding the spatial and temporal dynamics of

¹Department of Earth and Space Science, University of Washington, Seattle, Washington, USA.

²Department of Geological Sciences, Central Washington University, Ellensburg, Washington, USA.

Cascadia subduction. Tighter constraints on the slow slip source region could facilitate better spatial estimates of the freely slipping, transition, and locked segments of the subducting Juan de Fuca plate relative to the dense urban centers along the fault margin. Also, because slow slip transfers stress to the seismogenic portion of the plate interface, [e.g., *Rogers and Dragert, 2003; Mazzotti and Adams, 2004*], monitoring transient events may serve in forecasting the threat of a megathrust earthquake by inferring the temporal and spatial variations in the loading of the seismogenic zone.

[5] Increased GPS instrumentation allows for improved imagery of the slow slip region from geodetic inversions. Still, required smoothing limits the resolution of these inversions. The resolution of the GPS array to detect the distribution of slip along the plate interface is limited to the general distribution of slip over distances of roughly 25 km. Slip heterogeneity at shorter distances is obscured by the elastic smoothing of the overlying crust as well as the regularization required for stable inversion of the slip-deformation matrix [*Szeliga et al., 2008*]. As a result, tremor epicenters promise to be the best hope for a high-resolution map of the slow slip region. However, while the recurring spatial and temporal correlation suggests a close link between these two separate phenomena, it does not require their descriptions to be synonyms for the same source process. Nevertheless, in addition to the spatiotemporal correlation between tremor and slow slip [*Rogers and Dragert, 2003*], evidence from low-frequency earthquakes comprising tremor in Japan [*Shelly et al., 2007; Ide et al., 2007a*] and polarization analysis of tremor in Cascadia [*Wech and Creager, 2007*] suggests tremor and slow slip are manifestations of the same shear process. Furthermore, comparisons between geodetically estimated moment and the amount of tremor suggests that tremor may serve as a reliable proxy for slow slip [*Hiramatsu et al., 2008; Aguiar et al., 2009*]. Thus despite active debates over the depths [*Kao et al., 2005; McCausland et al., 2005; La Rocca et al., 2009*] and mechanism [*McCausland et al., 2005; Wech and Creager, 2007*] of Cascadia tremor, if this relationship holds, tremor epicenters provide a detailed map of the slow slip region.

[6] Though macroscopic spatial and temporal correlations have been identified [*Rogers and Dragert, 2003; Szeliga et al., 2008; McCausland et al., 2005; Brudzinski and Allen, 2007*], a detailed comparison has not been reported due to the inherent difficulties in locating tremor. Tremor has been successfully located in this region [*Kao et al., 2005; McCausland et al., 2005; Kao et al., 2007*], but high costs in computation time or labor associated with these techniques have made producing a complete tremor catalog difficult. Using a tremor autodetection and autolocation method [*Wech and Creager, 2008*], we present a more complete catalog of fifteen thousand tremor epicenters from the July 2004, September 2005, January 2007 and May 2008 ETS episodes and the February 2007–April 2008 inter-ETS time window. These results strengthen the correlation between slow slip and tremor by creating a high-resolution image of the slow slip region showing a strong first-order along strike correlation between peaks in slip and tremor density, and provide evidence of additional stable

sliding outside ETS episodes that may bleed off the remaining strain accumulation in the slow slip region.

2. Seismic Data and Methods

[7] Tremor epicenters were automatically detected and located by employing a cross-correlation method to generate potential epicenters before using the resulting epicenters to detect tremor [*Wech and Creager, 2008*]. By automatically analyzing network coherence through epicentral reliability and spatial repeatability, this method simultaneously locates and obviates the labor-intensive human efforts in detecting tremor. Based on data availability and quality, each ETS episode was analyzed with slightly different data sets. Using data from Pacific Northwest Seismic Network (PNSN) (2004–2008 ETS), Pacific Geoscience Centre (PGC) (2008 ETS), and EarthScope/Plate Boundary Observatory (PBO) borehole seismometers (2005–2008 ETS), and Earthscope Temporary Array and CAFE seismometers (2007 ETS), we choose a subnet comprising about 20 stations in western Washington and southern Vancouver Island based on geographic distribution and tremor signal-to-noise ratios.

[8] Locations are estimated using a cross-correlation method that maximizes tremor signal coherency among seismic stations. For a given 5-minute time window of vertical-component data, we bandpass filter from 1 to 8 Hz, create envelope functions, low-pass filter at 0.1 Hz, and decimate to 1 Hz. We obtain centroid location estimates by cross correlating all station pairs and performing a three-dimensional grid search over potential source location S-wave lag times that optimize the cross correlations. Thus for each grid location, \mathbf{x}^{grid} , and station pair $i-j$ we calculate the differential S-wave traveltime between the two stations, $\delta t_{ij}(\mathbf{x}^{\text{grid}})$, and evaluate the corresponding correlation value from the cross correlogram $C_{ij}(\delta t_{ij}(\mathbf{x}^{\text{grid}}))$. The weighted sum of these values for all station pairs is then maximized to determine the source location. Weights for each station pair are based on the maximum correlation for that pair. Using bootstrap error analysis and comparisons with earthquake locations, we estimate that our epicentral errors are up to 8 km with larger depth errors. See *Wech and Creager [2008]* for details on location, weights and error estimates.

3. Geodetic Methods

[9] The growing density of GPS stations allows the distribution of slip from each transient to be formally estimated from GPS deformation. In this formulation, we specify the plate boundary surface by linearly interpolating between depth contours specified by *Fluck et al. [1997]*. This surface is then divided into variable sized subfaults whose typical dimensions are around 25 km along strike and 15 km downdip. Exact subfault dimensions vary with geometry [*Szeliga et al., 2008*]. Three dimensional geometry dominated by the bend in the subducting plate mandates that each subfault be independently specified with a unique local strike, dip and rake, in addition to its along-strike and downdip length.

[10] Inverting for slip amounts to solving $G\mathbf{s} = \mathbf{d} + \boldsymbol{\varepsilon}$ where G is a Jacobian matrix of Green's functions relating surface displacement to a unit of pure thrust fault slip, \mathbf{s} is the vector of dip-slip slip at each subfault, \mathbf{d} is the observed

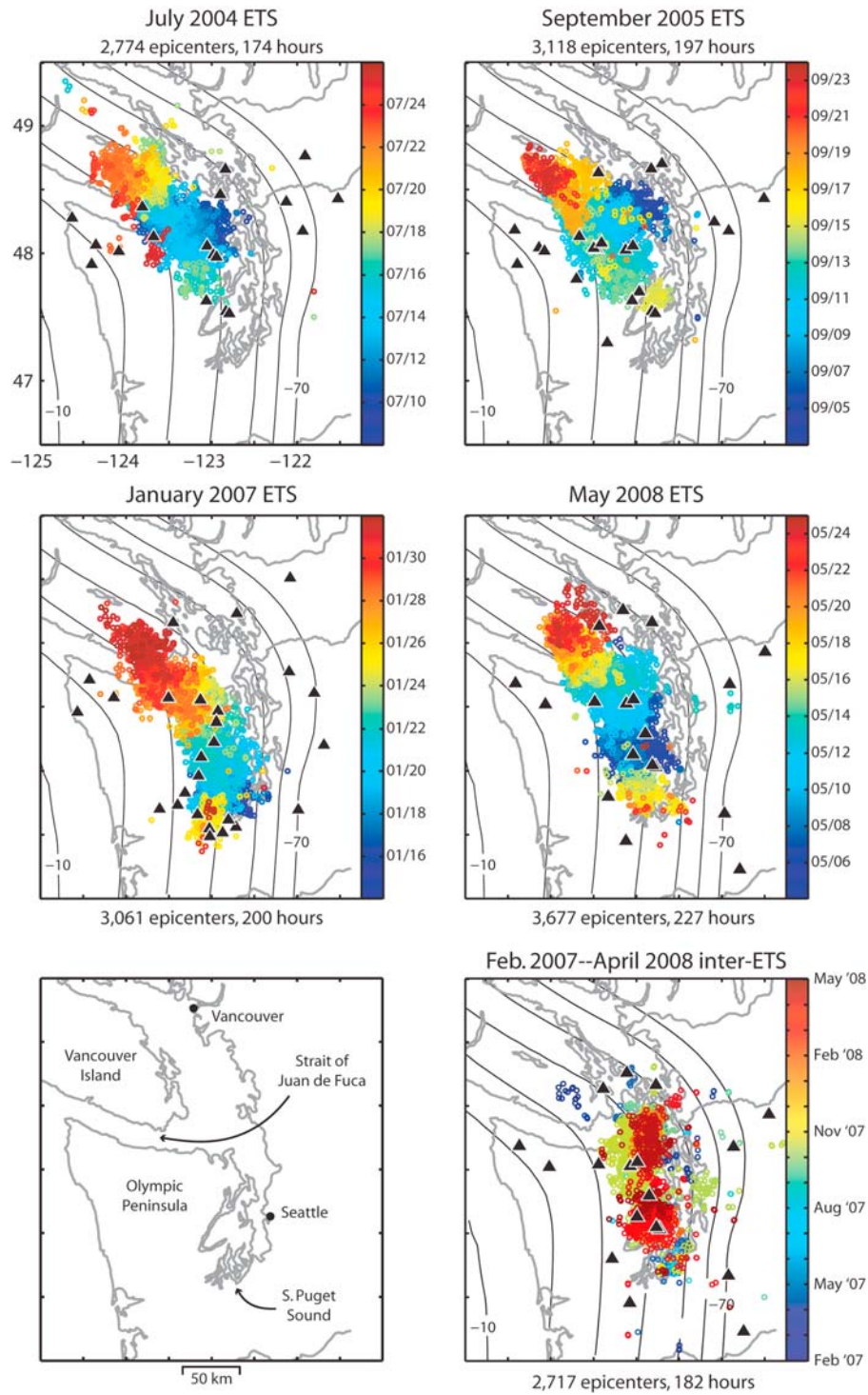


Figure 1. Tremor epicenters (circles color coded by time) from four ETS episodes and one 15-month inter-ETS interval, station distribution (triangles), and plate interface geometry (contoured at 10-km intervals) from *McCrorey et al.* [2004].

vector of north, east and vertical slow-slip event offsets, weighted by their formal uncertainties, for each GPS station recording an event and ϵ is the error. The number of unknown model parameters greatly exceeds the number of observations so additional information is required to reduce the nonuniqueness and stabilize the inversion. We apply

both positivity and solution smoothness constraints in our inversion process [*Szeliga et al.*, 2008].

4. ETS Tremor Descriptions

[11] For each ETS episode only those epicenters with error estimates under 5 km that cluster in space and time (2

Table 1. Tremor (Columns 2–4) and Geodetic Slip (Columns 5–6) Information for Each ETS Episode and One Inter-ETS Episode^a

Event	Number of Epicenters	Duration (hrs)	Migration (km/day)	Slip (cm)	M _w
July 2004	2774	174	11	2.3	6.6
September 2005	3118	197	12	3.1	6.7
January 2007	3061	200	9	3.9	6.6
May 2008	3677	227	13	2.9	6.5
February 2007–April 2008	2717	182	11	NA	NA

^aDuration assumes each epicenter detection represents 5 minutes of tremor and accounts for window overlap.

or more locations per 0.1×0.1 degree per day) are determined to represent tremor [Wech and Creager, 2008]. Figure 1 shows epicenters color-coded by time to show migration. Epicenters are only tracked up to southernmost Vancouver Island and south Puget Sound (Figure 1), after which they are beyond our network coverage. Timescales vary according to the beginning and end of each event. Despite variable station coverage, each episode yielded similar numbers of epicenters and durations (summing the number of epicenters, but accounting for overlap) (Table 1).

[12] For the July 2004 ETS we detect 174 hours of tremor and 2,774 epicenters. Tremor began on 8 July in the eastern Strait of Juan de Fuca. Averaging 11 km/day, tremor bursts spread west over the next 7 days throughout the straits to just south of southern Vancouver Island before splitting and heading southeast (ending on 17 July) and northwest (ending about 23 July) with a late burst occurring in the northern Olympic Peninsula on 25 July (Figure 1).

[13] For the September 2005 ETS we detect 197 hours of tremor and 3,118 epicenters. Tremor began on 3 September (Figure 1), east of Vancouver Island. During the next ten days at a rate of 12 km/day, tremor epicenters migrated to the southwest, stalling beneath the northern shore of the Olympic Peninsula before bifurcating and heading southeast (ending on 15 September) and northwest (ending about 30 September) as seen by Wech and Creager [2007].

[14] For the January 2007 ETS we detect 200 hours of tremor and 3,061 epicenters. Migrating at 9 km/day from central Puget Sound to Vancouver Island from 14 to 31 January and then North beyond our network's border, with a late cluster occurring in southern Puget Sound on 25–31 January (Figure 1).

[15] For the May 2008 ETS we detect 227 hours of tremor and 3,677 epicenters migrating from central Puget Sound to Vancouver Island from 4 to 24 May at 13 km/day and then North beyond our network's border, with a late cluster occurring in southern Puget Sound on 15–17 May (Figure 1).

[16] Tremor migration varies among episodes, but common patterns can be seen between the 2004 and 2005 episodes. In each case, tremor began further updip prior to an updip, southwest migration that resulted in bifurcation and along strike migration to the north and south. This behavior is markedly different than the migrations of the 2007 and 2008 tremor episodes. Though latitudinally offset by about 20 km, in each of these latter cases tremor initiated in the south Puget Sound region, then migrated northward along strike with a late cluster reoccurring in the southern Puget Sound. Overall, each tremor pattern is approximately

20–25 km wide above where the plate interface is 30–45 km deep (Figure 1) and migrated at an average of 10–13 km/day (Table 1). The 2007 tremor pattern is notably narrower, which probably more accurately represents true map view constraints due to the higher data quality of the Earthscope CAFE data set. Epicenters from each episode have a well-resolved sharp updip boundary about 75 km east of current estimates of the downdip edge of the locked zone [McCaffrey et al., 2007] (Figure 1).

5. Tremor and Slip

[17] Equipped with a complete catalog of tremor epicenters for each ETS episode, we can compare the tremor source region with slow slip inversions. Combining these new slow slip geodetic inversions with complete tremor descriptions enables detailed spatial comparisons between tremor and slip. Figure 2 plots the contours of all tremor epicenters gridded into counts/ 0.1×0.1 degree bins for individual ETS events and compares these against the results of the slip inversions. For each of the 4 ETS episodes, tremor and slow slip are independently observed to occur in the same areas, with regions of high tremor density spatially correlating well with regions of concentrated slow slip (Figure 2). Specifically, the 2004 and 2005 events had tremor and slip concentrated in the north, while the 2005 event also exhibited weaker activity at about 48 N. In contrast, the 2007 and 2008 events slip further south, with an especially strong concentration of southern activity for the 2007 event. In each case, it appears that the slip distribution is a slightly smoothed version of the tremor distribution with broad slip peaks often averaging across adjacent high tremor features. This comparison confirms previous large-scale spatial correlations in Cascadia, but the increased number of tremor epicenters from a complete catalog confines ETS tremor to the slow slip region while strengthening the case for a close relationship between the two phenomena.

[18] Figure 3 shows contours from the combination of all tremor epicenters from the past 4 ETS episodes and compares this ETS tremor map against the slow-slip sum from the same 4 ETS episodes. As seen in the individual cases above, there is a strong 1st-order spatial correlation between the regions of high tremor activity and increased slow slip. However, what stands out over the longer term is a sharp updip boundary in the middle of the Olympic Peninsula seen in the tremor density contours (Figures 3 and 5). This updip edge is seen more easily with tremor than slip (likely because of the smoothing required for geodetic inversions), is more prominent in the north, and appears to be spatially correlated with the northern coastline of the Olympic Peninsula (Figure 3). Given the varying seismic subnets from episode to episode and the station coverage updip of this edge, the resulting edge is likely a real feature; and, because of the uncertainties in tremor epicenters, this boundary may be even sharper than indicated. This edge, therefore suggests an ETS boundary that may be the signature of a change in plate interface conditions such as fluid pressure or reflect a change in the rheology of the overriding material.

[19] Despite good 1st order agreement, there are two notable differences. Improved geodetic resolution is likely

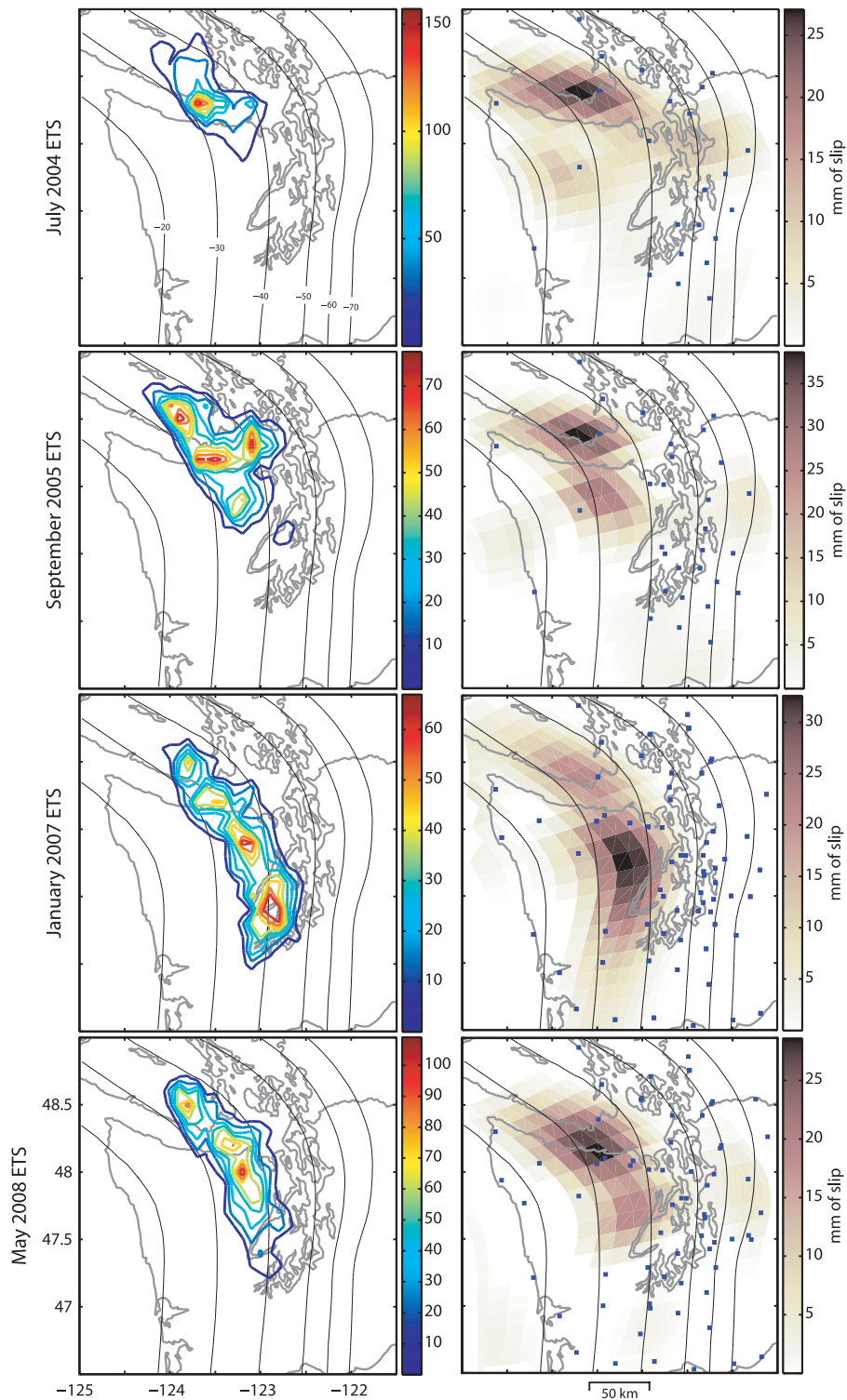


Figure 2. (left) Sum of all tremor epicenters per 0.1 by 0.1 degree bin compared with (right) geodetic slip estimates for each of the four most recent ETS episodes. Blue squares represent the GPS stations used for each inversion (only the those within this map view are shown). Plate interface geometry (contoured at 10-km intervals) from *McCrory et al.* [2004].

needed to scrutinize the slight differences between individual peaks in single ETS episodes; however, it is worth noting overall discrepancies. First, tremor is in some areas shifted downdip of slow slip estimates. This shift is most pronounced in region 1 where we observe up to a 20 km

discrepancy (Figures 3 and 5), but may be the result of this study’s limited seismic coverage up into Vancouver Island. Regions 3 and 4 show a smaller downdip offset of ~10 km (Figures 3 and 5). If this offset is real, ETS models would need to explain slip occurring updip of tremor. However, the

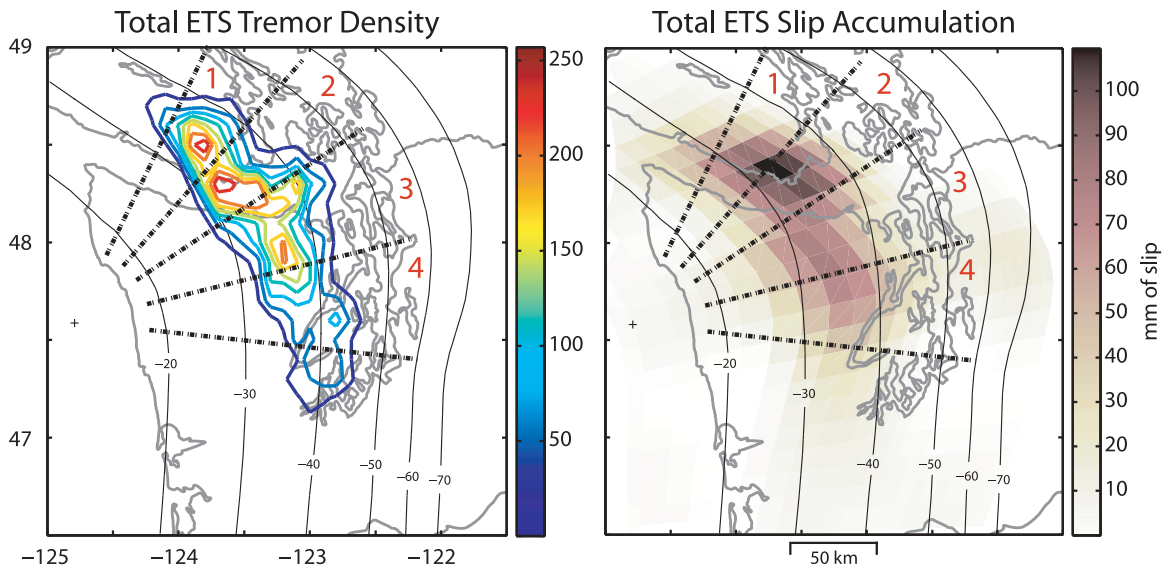


Figure 3. (left) Sum of all tremor epicenters per 0.1 by 0.1 degree bin and (right) sum of plate-interface slip over 4 ETS episodes. Black dashed lines demarcate regions analyzed in Figure 5. Plate interface geometry (contoured at 10-km intervals) from the work of *McCrorry et al.* [2004].

region to most heavily scrutinize is region 2, where the most slip and the most tremors are observed. In this region, the tremor and slip peaks line up exactly (Figure 3 and 5) and strongly support the idea that tremor and slip are different observations of the same process. Second, the slip distributions are broader than the tremor distributions. This is likely an artifact of seeking the smoothest slip distribution that fits the GPS data. An important consequence of this is that if the slip is forced into a smaller area, the GPS data would require more slip, possibly accounting for a much greater portion of the relative plate motion.

[20] Ultimately, more observations, more comparisons and improvements in seismic and geodetic methodologies are required to determine the significance of the aforementioned discrepancies. Macroscopically, however, we find a good agreement between tremor epicenters and slow slip estimates. A two-dimensional cross correlation of total tremor and total slip yielded a correlation value of 0.83 with tremor latitudinally and longitudinally offset by 2 km north and 11 km east respectively. When combined with the profile agreement seen where the most of the tremor and slip occur (region 2 of Figure 5), this correlation supports a model causally connecting tremor and slip.

6. Inter-ETS Tremor

[21] Monitoring inter-ETS tremor by hand has shown that there are many bursts of tremor with no associated geodetic signal [*McCausland et al.*, 2005]; however, there has been very little location work and no complete catalog has yet characterized an inter-ETS time window. Our automated tremor detection and location algorithm afforded the opportunity to perform a detailed tremor study of one inter-ETS period. During the 15 months between the January 2007 and May 2008 ETS episodes, we identify and locate numerous ageodetic tremor bursts [*Wech and Creager*, 2008]. We keep the tremor detections with bootstrap errors less than 5 km

and that cluster in space and time to avoid noise and earthquakes. We obtain 182 hours of inter-ETS tremor and 2,717 epicenters from the February 2007–April 2008 inter-ETS period (Figure 4). Each individual swarm lasted for one to seven days and typically migrated along strike at 11 km/day (Table 1). These tremors occur in the slow slip region, spatially compliment ETS tremor (Figure 4), and account for approximately 45% of the total tremor duration detected during the entire ETS cycle [*Wech and Creager*, 2008]. However, these inter-ETS locations show some different spatial characteristics from the previous 4 ETS tremor locations. For example, the peak of the distribution of inter-ETS tremor is downdip of the peaks during ETS, lying above plate depths of 40–45 km versus 33–38 km for ETS tremor (Figures 4 and 5). Furthermore, these inter-ETS tremor locations also appear to be spatially limited along strike. Specifically, they do not extend north beyond 48.5°N and south beyond 47.5°S. We think both observations are real, but interpreting them is difficult to do with just one inter-ETS observation. In fact, since the May 2008 episode and first drafting this paper, our methodology has detected inter-ETS tremor north of 48.5°N, and south of 47.5°S.

7. Implications

[22] With our tremor catalog we have provided a detailed description of tremor activity in space and time during each of the last 4 ETS episodes and shown new complete evidence of a tight spatial correlation between episodic tremor and slip. Comparing the spatial extent of the tremor source region with slip inversions strengthens the correlation between tremor and slip, and taking this correlation a step further highlights the utility of having a detailed description of tremor.

[23] The tremor and slip spatial correlations of each individual ETS episode and their total accumulations provide strong evidence that tremor can be used to monitor slip.

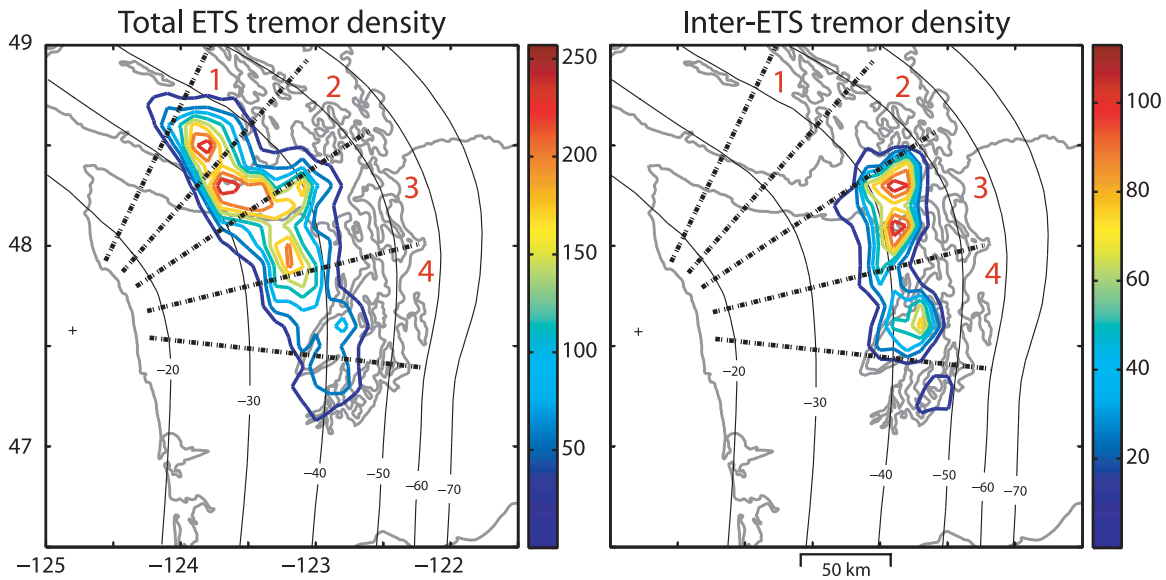


Figure 4. Sum of all tremor epicenters per 0.1 by 0.1 degree bin (left) for all four ETS episodes and (right) for one inter-ETS period. Note these time periods are mutually exclusive. Black dashed lines demarcate regions analyzed in Figure 5. Plate interface geometry (contoured at 10-km intervals) from the work of *McCrory et al.* [2004].

Alone this evidence does not establish a one to one correlation between the two phenomena. However, when put together with previous tremor and slip results from Japan and Cascadia [*Shelly et al.*, 2007; *Ide et al.*, 2007a; *Wech and Creager*, 2007], we argue that our tremor epicenters monitor and map slow slip, even when the amount of slip is below the current GPS detection levels. Evidence from the two most studied ETS regions, southwest Japan and northern Cascadia, suggests in several ways that tremor is a proxy for slip. Estimated seismic moment from Japan tremor and total duration from Cascadia tremor have been observed to be proportional to the size of corresponding slow slip episodes [*Hiramatsu et al.*, 2008; *Aguiar et al.*, 2009]. Japanese tremor appears to be composed of low-frequency earthquakes that represent thrust on the plate interface during slow slip events [*Shelly et al.*, 2007; *Ide et al.*, 2007a]. In Cascadia analysis of tremor polarization [*Wech and Creager*, 2007] combined with recent tremor depth estimates [*La Rocca et al.*, 2009] lead to the same conclusion. These results combined with our spatial correlations suggest that Cascadia tremor occurs on the plate interface with a thrust mechanism associated with slow slip. Therefore we interpret tremor and slip as different observations of the same physical process but on opposite ends of the frequency spectrum [*Ide et al.*, 2007b], a spectrum that is slowly filling in. The timescale gap between tremor observed at frequencies above 1 Hz and slow slip observed over many days is beginning to be filled in with observations from southwest Japan of slow events radiating energy at periods of 20 seconds [*Ito et al.*, 2007] and 200 seconds [*Ide et al.*, 2008].

[24] This interpretation thus allows us to map the slow slip region and use tremor epicenters to monitor slow slip occurrences. By extrapolating the spatial and temporal correlation between the two phenomena, tremor epicenters can supplement geodetic spatial constraints of the slow slip

region. Tremor epicenters provide a high resolution map of the slow slip region, reinforced and quantified by GPS observations.

8. Conclusions

[25] Ultimately this leads us to three important conclusions. (1) Thousands of epicenters from each of the past four ETS events provide detailed map-view tremor constraints that correlate well with geodetic estimates of the simultaneous slow slip. This agreement provides additional evidence that tremor and slip are different observations of the same phenomenon. (2) Combining these epicenters from all four ETS episodes provides a high-resolution map of the slow-slip region (Figure 3) which maps a region of strain release to accommodate the northeasterly 4 cm/a convergence of the subducting Juan de Fuca plate beneath North America. Our epicenters show evidence of a sharp updip edge to the slow-slip region, and we interpret this boundary to represent a change in the physical properties at the plate interface that inhibits updip ETS-like behavior. (3) Comparable amounts of tremor detected between versus during ETS episodes provides evidence of significant stable sliding outside of major, GPS-observed slow-slip events. We suggest that ageodetic, inter-ETS tremor represents slip which is relieving strain accumulation from plate convergence. Together with the updip edge observed with the past cumulative ETS tremor and the growing understanding that tremor and slip are the same phenomena, this result implies slow slip occurs in the freely slipping region and tremor epicenters demarcate the downdip edge of the transition zone.

[26] This last conclusion requires a couple of considerations. Finding 45% of tremor activity during an ETS cycle to occur between ETS events could suggest that the mapped slow slip region is, in the long term, accommodating all of

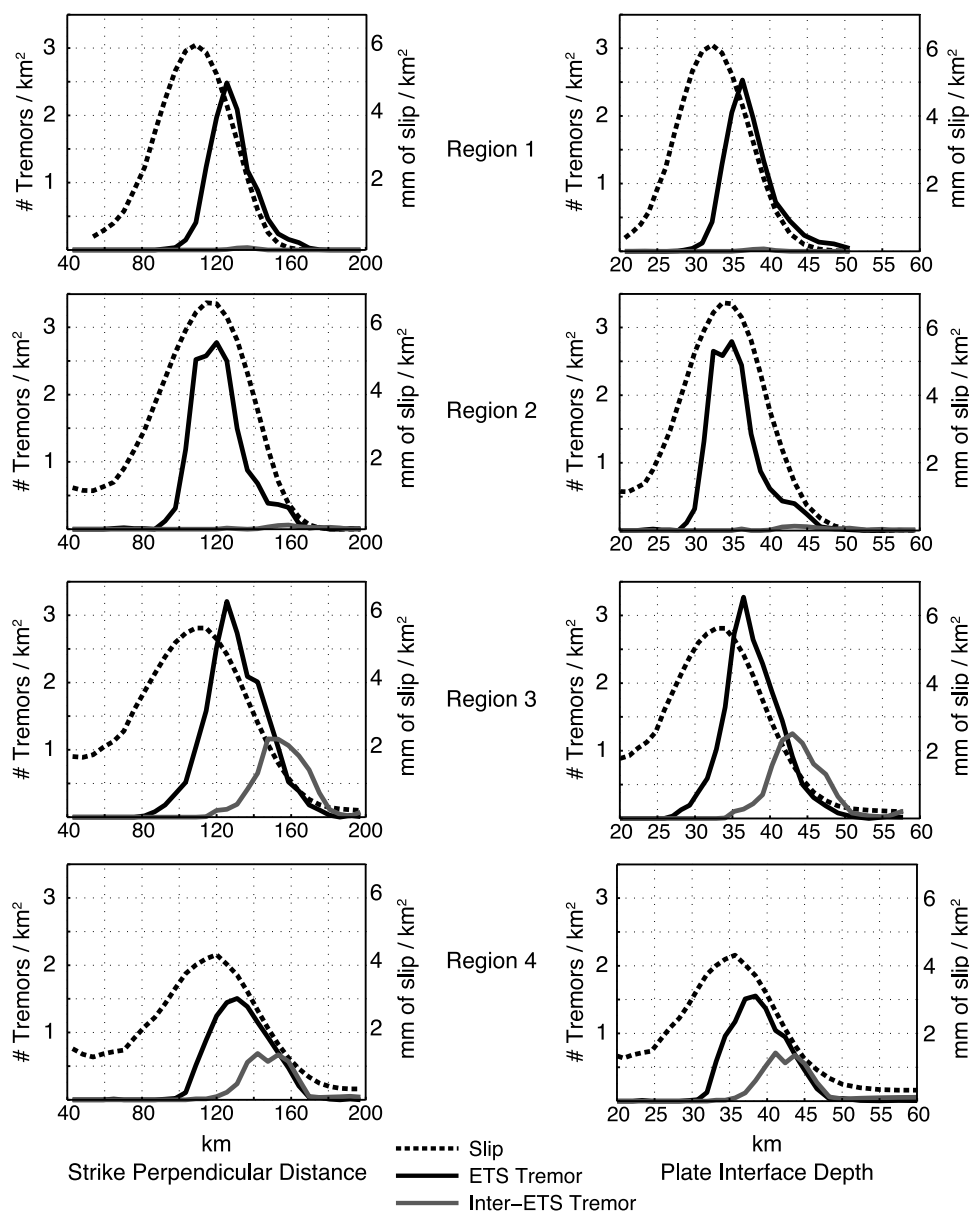


Figure 5. Profiles of ETS tremor (solid black line), inter-ETS tremor (solid gray line), and slip (dashed line) densities for four along-strike regions shown in Figures 3 and 4. The number of tremor locations/ km^2 for each strike-perpendicular bin are plotted against the left y axis. The average slip in mm/km^2 for each strike-perpendicular bin is plotted against the right y axis. The x axis corresponds to (left plots) strike-perpendicular distance from a reference point and (right plots) plate interface depth.

the relative plate motion. With typical slip of 2–3 cm every 15 months, ETS only accounts for 45–65% of the plate convergence rate of 4 cm/a. Perhaps the 45% of tremor occurring between ETS events, which we interpret to represent slip at levels below current GPS resolution, accommodates the remaining strain build up.

[27] However considering that inter-ETS tremor was observed downdip of the ETS region, it is possible that rather than temporally accommodating the remaining slip deficit in the ETS region over time, inter-ETS tremor may represent a spatial accommodation of plate convergence. The large strike-perpendicular width of slip estimates versus tremor counts (Figure 5) suggest that we may be underestimating slow slip. Confining all the slip to the tremor

region may bring slip estimates in the ETS zone closer to a balanced slip budget, in which case inter-ETS tremor is accommodating a spatial slip deficit, not a temporal one. Of course, we have only had the opportunity to study one inter-ETS period, and the repeatability of inter-ETS tremor totals and locations relative to ETS tremor are critical in properly interpreting inter-ETS plate coupling. Certainly more observations of the entire ETS cycle will help resolve which, if either, of these interpretations is correct.

[28] Nevertheless, if tremor does account for all of the converging plate motion, it raises an important question about how stress is released updip of the sharp ETS boundary and downdip of the seismogenic zone. It is possible that slip might be accommodated by continuous

slip, coseismic shear failure during a megathrust earthquake, postseismic afterslip associated with a megathrust rupture, large slow-slip events with repeat intervals longer than continuous GPS has been available, or some combination of all of these. By further constraining this transition zone with more ETS and inter-ETS observations using increased instrumentation and higher quality data, we can begin to answer this question and gain a better understanding of the downdip seismic hazards posed by a megathrust rupture.

[29] **Note Added in Proof.** Analysis using a different station set, but similar methods, suggests that tremor during the 2007 and 2008 ETS events (and possibly others) continues further south than shown in Figure 1.

[30] **Acknowledgments.** This work was supported by the National Science Foundation and the United States Geological Survey. Primary seismic data were supplied by PNSN, PGC, and the Earthscope Flexible Array, Transportable Array and Plate Boundary Observatory. We thank R. Crosson for his envelope processing. We also thank J. Vidale, A. Ghosh, and J. Sweet for valuable discussion, as well as two anonymous reviewers for constructive comments. Finally, a special nod to tallboy:30 and its associated cast members for inspiration.

References

- Aguiar, A. C., T. I. Melbourne, and C. W. Scrivner (2009), Moment release rate of Cascadia tremor constrained by GPS, *J. Geophys. Res.*, *114*, B00A05, doi:10.1029/2008JB005909.
- Brudzinski, M. R., and R. M. Allen (2007), Segmentation in episodic tremor and slip all along Cascadia, *Geology*, *35*, 907–910, doi:10.1130/G23740A.1.
- Dragert, H., K. Wang, and T. S. James (2001), A silent slip event on the deeper Cascadia subduction interface, *Science*, *292*, 1525–1528, doi:10.1126/science.1060152.
- Fluck, P., R. Hyndman, and K. Wang (1997), Three-dimensional dislocation model for great earthquakes of the Cascadia subduction zone, *J. Geophys. Res.*, *102*(B9), 20,539–20,550.
- Goldfinger, C., et al. (2003), Holocene earthquake records from the Cascadia subduction zone and northern San Andreas Fault based on precise dating of offshore turbidities, *Annu. Rev. Earth Planet. Sci.*, *31*, 555–577.
- Hiramatsu, Y., T. Watanabe, and K. Obara (2008), Deep low-frequency tremors as a proxy for slip monitoring at plate interface, *Geophys. Res. Lett.*, *35*, L13304, doi:10.1029/2008GL034342.
- Ide, S., D. R. Shelly, and G. C. Beroza (2007a), Mechanism of deep low frequency earthquakes: Further evidence that deep non-volcanic tremor is generated by shear slip on the plate interface, *Geophys. Res. Lett.*, *34*, L03308, doi:10.1029/2006GL028890.
- Ide, S., G. C. Beroza, D. R. Shelly, and T. Uchide (2007b), A scaling law for slow earthquakes, *Nature*, *447*, 76–79, doi:10.1038/nature05780.
- Ide, S., K. Imanishi, Y. Yoshida, G. C. Beroza, and D. R. Shelly (2008), Bridging the gap between seismically and geodetically detected slow earthquakes, *Geophys. Res. Lett.*, *35*, L10305, doi:10.1029/2008GL034014.
- Ito, Y., K. Obara, K. Shiomi, S. Sekine, and H. Hirose (2007), Slow earthquakes coincident with episodic tremors and slow slip events, *Science*, *315*, 503–506.
- Kao, H., S. Shan, H. Dragert, G. Rogers, J. F. Cassidy, and K. Ramachandran (2005), A wide depth distribution of seismic tremors along the northern Cascadia margin, *Nature*, *436*, 841–844, doi:10.1038/nature03903.
- Kao, H., P. J. Thompson, G. Rogers, H. Dragert, and G. Spence (2007), Automatic detection and characterization of seismic tremors in northern Cascadia, *Geophys. Res. Lett.*, *34*, L16313, doi:10.1029/2007GL030822.
- Kodaira, S., T. Iidaka, A. Kato, J. Park, T. Iwasaki, and Y. Kaneda (2004), High pore fluid pressure may cause silent slip in the Nankai Trough, *Science*, *304*, 1295–1299, doi:10.126/science.1096535.
- La Rocca, M., K. C. Creager, D. Galluzzo, S. Malone, J. E. Vidale, J. R. Sweet, and A. G. Wech (2009), Cascadia tremor located near plate interface constrained by S minus P times, *Science*, *323*, 620–623, doi:10.1126/science.116711.
- Mazzotti, S., and J. Adams (2004), Variability of near-term probability for the next great earthquake on the Cascadia subduction zone, *Bull. Seismol. Soc. Am.*, *94*, 1954–1959.
- McCaffrey, R., A. I. Qamar, R. W. King, R. Wells, G. Khazaradze, C. A. Williams, C. W. Stevens, J. J. Vollick, and P. C. Zwicker (2007), Fault locking, block rotation and crustal deformation in the Pacific Northwest, *Geophys. J. Int.*, *169*(3), 1315–1340.
- McCausland, W., S. Malone, and D. Johnson (2005), Temporal and spatial occurrence of deep non-volcanic tremor: From Washington to northern California, *Geophys. Res. Lett.*, *32*, L24311, doi:10.1029/2005GL024349.
- McCrory, P. A., J. L. Blair, D. H. Oppenheimer, and S. R. Walter (2004), Depth to the Juan de Fuca slab beneath the Cascadia subduction margin: A 3-D model for sorting earthquakes, *U. S. Geol. Surv. Data Ser.*, *91*, 1–13.
- Miller, M. M., T. Melbourne, D. J. Johnson, and W. Q. Sumner (2002), Periodic slow earthquakes from the Cascadia Subduction Zone, *Science*, *295*, 2423.
- Obara, K. (2002), Nonvolcanic deep tremor associated with subduction in Southwest Japan, *Science*, *296*, 1679–1681.
- Rogers, G., and H. Dragert (2003), Episodic tremor and slip on the Cascadia subduction zone: The chatter of silent slip, *Science*, *300*, 1942–1943, doi:10.1126/science.1084783.
- Satake, K., K. Wang, and B. F. Atwater (2003), Fault slip and seismic moment of the 1700 Cascadia earthquake inferred from Japanese tsunami descriptions, *J. Geophys. Res.*, *108*(B11), 2535, doi:10.1029/2003JB002521.
- Shelly, D. R., G. C. Beroza, S. Ide, and S. Nakamura (2006), Low-frequency earthquakes in Shikoku, Japan, and their relationship to episodic tremor and slip, *Nature*, *442*, 188–191, doi:10.1038/nature04931.
- Shelly, D. R., G. C. Beroza, and S. Ide (2007), Non-volcanic tremor and low-frequency earthquake swarms, *Nature*, *446*, 305–307, doi:10.1038/nature05666.
- Szeliga, W., T. Melbourne, M. Santillan, and M. Miller (2008), GPS constraints on 34 slow slip events within the Cascadia subduction zone, 1997–2005, *J. Geophys. Res.*, *113*, B04404, doi:10.1029/2007JB004948.
- Wech, A. G., and K. C. Creager (2007), Cascadia tremor polarization evidence for plate interface slip, *Geophys. Res. Lett.*, *34*, L22306, doi:10.1029/2007GL031167.
- Wech, A. G., and K. C. Creager (2008), Automatic detection and location of Cascadia tremor, *Geophys. Res. Lett.*, *35*, L20302, doi:10.1029/2008GL035458.
- Wilson, D. S. (1993), Confidence intervals for motion and deformation of the Juan de Fuca Plate, *J. Geophys. Res.*, *98*(B9), 16,053–16,071.

K. C. Creager and A. G. Wech, Department of Earth and Space Science, University of Washington, Box 351310, Seattle, WA 98195, USA. (wech@u.washington.edu)

T. I. Melbourne, Department of Geological Sciences, Central Washington University, 400 E. University Way, Ellensburg, WA 98926, USA.